Potential-Induced Degradation (PID): Incomplete Recovery of Shunt Resistance and Quantum Efficiency Losses

Jaewon Oh, Stuart Bowden, and GovindaSamy TamizhMani

***Abstract*—Potential-induced degradation (PID), specifically PID leading to shunts (PID-s), has recently been identified as one of the major field durability issues of photovoltaic (PV) modules. The industry is attempting to address this issue at the module/cell production level by modifying the cell, glass, and/or encapsulant properties, as well as at the system level through the application of reverse potential at night. However, there is a lingering question on the full recovery of the cells through the reverse potential application technique. The results obtained in this study indicate that the near-full recovery of efficiency at high irradiance levels can be achieved, but the full recovery of efficiency at low irradiance levels, shunt resistance, and quantum efficiency (QE) at low wavelengths could not be achieved. The wavelength-dependent QE response after PID and recovery has been modeled based on experimental data. We address the challenge in measuring accurate QE of shunted cells and the input impedance of traditional QE test equipment. A new very low impedance method minimizes, but does not totally eliminate, the scaling error in the QE system data for solar cells that have very low shunt resistances. We also evaluate previously proposed models on the effects of sodium experimentally and through simulation.**

***Index Terms*—Durability, high voltage, potential-induced degradation (PID), quantum efficiency (QE), reliability, shunt resistance.**

I. Introduction

ONE of the high-voltage stress-based performance-loss issues experienced by photovoltaic (PV) modules in the field is called potential-induced degradation (PID) [1]. It has been observed that PID-stressed PV modules have shown significant output power decrease (∼30%), even more at low irradiance level, and an increase of hot-spot risk [1]–[3]. In response to this field issue, a new IEC standard for PID is being developed [4], [5]. This degradation is mainly due to a cell junction shunting [6]–[9]; therefore, the PID is more specifically called PID of the shunting type (PID-s) [8], [9] in order to discriminate from the other PID, such as electrochemical corrosion [10]. Sodium has been suspected to cause PID [6], as well as source of sodium identified in the PV module glass [11], which is usually soda-lime glass. It has been shown that sodium-decorated stacking faults located from the cell surface through junction lead to shunting through a thin quasi-metallic layer [8], [9], [12]. The PID/PID-s has only been observed with p-base crystalline silicon (c-Si) cells negatively biased to the frame. This issue could technically be addressed at the cell/module manufacturing level or at the installed system level. At the manufacturing level, the PID issue can be addressed by modifying the silicon nitride antireflection coating [1], [2], by preventing ion conduction through encapsulant or by eliminating sodium content in the glass superstrate [11], [13]. If the system is already installed in the field with PID susceptible cells/modules, the PID issue can still be addressed by applying a reverse potential on the modules during the nighttime [7], [14] so that the cells are positively biased to the frame. Since the energy consumption during this recovery period is so small, when compared with the energy production during the daytime, the reverse-potential approach to address the PID issue has been implemented by many system owners. However, recent papers separately discuss an incomplete recovery under reverse potential in terms of efficiency at high and low irradiance levels, shunt resistance of cells, and the quantum efficiency (QE) [6], [14], [15]. Moreover, QE measurement on PID-stressed cells has yet to be thoroughly investigated, although QE loss at short wavelength was observed and briefly reported in PID-stressed cells by our research group [15], [16]. QE curves of solar cells are obtained by measuring the cell's light-generated current at various wavelengths when monochromatic light shines on the cell. This measured current is very sensitive to the cell's shunt resistance, and it may lead to scaling error when shunt resistance is very low in, for example, PID-stressed cells. In this paper, we present a detailed analysis on the effectiveness of the reverse-potential method on the recovery of the PID-subjected cells and incompleteness of QE recovery, which have been previously published [15], [16]. PID-affected QE curves based on QE loss at short wavelength have also been modeled in this paper. This paper also presents the challenges in measuring accurate QE of heavily shunted cells and the QE results obtained using a newly developed ultralow impedance accessory. Investigation of the source of sodium and the challenges with an alternate PID inversion model [17] is presented in last two sections of this paper.

Manuscript received February 18, 2015; revised April 23, 2015 and June 28, 2015; accepted July 15, 2015. This work was supported by the National Science Foundation (NSF) and the Department of Energy (DOE) under NSF CA No. EEC-1041895 and in part by DOE/SERIIUS. Any opinions, findings, and conclusions or recommendations expressed in this material are those of the author(s) and do not necessarily reflect those of NSF or DOE.

J. Oh and S. Bowden are with the Solar Power Laboratory, Arizona State University, Tempe, AZ 85284 USA (e-mail: jaewonoh@asu.edu; sgbowden@asu.edu).

G. TamizhMani is with the Photovoltaic Reliability Laboratory, Arizona State University, Mesa, AZ 85212 USA (e-mail: manit@asu.edu).

Color versions of one or more of the figures in this paper are available online at http://ieeexplore.ieee.org.

Digital Object Identifier 10.1109/JPHOTOV.2015.2459919

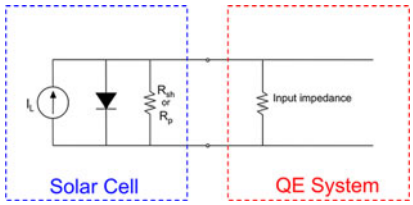

Fig. 1. Basic circuit diagram of a solar cell indicating shunt ($R_{\rm sh}$ or R_p) and input impedance of the QE system

II. Experiments

Test coupons (one-cell laminates) were constructed using common commercial-grade construction materials of glass, EVA, cell, and backsheet. The experiments were performed using 156 mm × 156 mm size p-base monocrystalline silicon cells, which are susceptible to the PID issue. The PID stress experiments were carried out at −600 V for 88 h at two different temperatures (60 °C and 85 °C) with 0% relative humidity (RH). The front glass was fully covered with an adhesive conductive aluminum tape to obtain uniform conductivity throughout the glass surface. The negative voltage was applied to the shorted leads of test cell coupon and the positive voltage was applied on the aluminum tape covering the front glass surface.

Before and after the PID test, all test samples were characterized by light *I–V* (LIV), dark *I–V* (DIV), electroluminescence (EL) imaging, infrared imaging (IR), and QE. A steady-state solar simulator was used to take the *I–V* measurements. The recovery experiments were carried out using a reverse potential of +600 V for 88 h at 60 °C, 0% RH. The reverse-potential-subjected samples were characterized using the techniques identified above and then stored at room temperature with no imposed potential and periodically characterized to observe additional recovery, if any. In addition, some of the PID-stressed samples that were not subjected to reverse-potential recovery were stored and periodically characterized at room temperature to compare the recovery rates between the reverse-potential samples and room temperature stored samples. The recovery rate and extent are reported in terms of power recovery at both high and low irradiances, shunt resistance recovery, and QE recovery at wavelengths between 350 and 1100 nm.

The QE measurement artifacts of heavily shunted cells can be simulated using an externally connected parallel resistors (R_p) as shown in Fig. 1. If the QE system input impedance is not exactly zero, a small voltage drop will develop at the QE system connection, driving current through the external R_p instead of to the QE system to be measured. Thus, the measured QE decreases. This wavelength-independent scaling error in QE can be significantly reduced by utilizing a very low impedance method. A new ultralow impedance accessory developed by PV Measurements, Inc., has been utilized in the QE system of this work to minimize the QE drops of the heavily shunted cells.

III. Results and Discussion

A. Incomplete Recovery of Power and Shunt Resistance

Fig. 2(a) shows the progress of PID and recovery of maximum power ($P_{\rm max}$) at 1000 W/m^2 and on shunt resistance. After 88 h of PID stress at 60 °C, the remaining power was determined to be 70% when compared with the initial power, and the shunt resistance dropped to under 1 Ω. After the PID test, the sample was stored at room temperature with no potential for more than 75 days, and the power at 1000 W/m^2 is determined to be recovered to about 92%. However, the recovery of shunt resistance is still very low although most of the power at this high irradiance level is recovered.

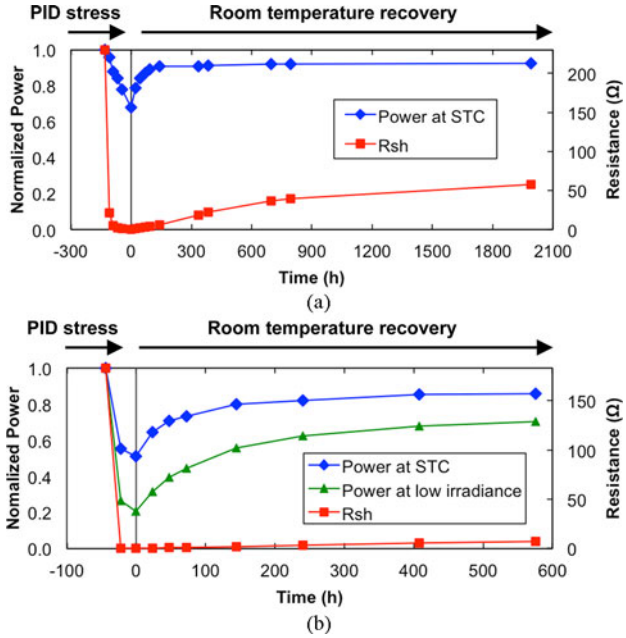

Fig. 2. (a) Recovery rate and level of output power at high (1000 W/m^2) irradiance level and shunt resistance during the recovery period at room temperature (no aluminum and no bias for 1992 h) on a test sample subjected to the PID stress at **60 °C/0%RH** (aluminum covered, −600 V, 88 h). (b) Recovery rate and level of output power at high (1000 W/m^2) and low (240 W/m^2) irradiance levels and of shunt resistance during the recovery period at room temperature (no aluminum and no bias for 576 h) on a test sample subjected to the PID stress at **85 °C/0% RH** (aluminum covered, −600 V, 44 h).

At 85 °C PID stress, a much higher power drop in a shorter time of test was observed as shown in Fig. 2(b). After leaving at room temperature for more than 500 h, the recovered power was only 87% at 1000-W/m^2 irradiance level and 60% at 240-W/m^2 irradiance level, and the recovered shunt resistance is practically insignificant. In addition, it takes much longer for both $P_{\rm max}$ and shunt resistance to be recovered when compared with the 60 °C PID-stressed samples due to extensive damage to the cell materials and/or junction, which may not be a realistic observation in the field.

To observe if an applied reverse voltage at a higher temperature than the room temperature could recover the cells to a higher level, another set of test coupons were prepared and subjected to the tests as shown in Fig. 3. There is practically no difference in recovery of power at 1000-W/m^2 irradiance level, between 0 and +600 V potential, but the reverse potential at high temperature accelerates recovery from PID in a shorter amount of time compared with room temperature storage with no voltage application, as described in [14]. Even though the recovery of power at high irradiance of 1000 W/m^2 is as high as 93% of its original, the recovery of the shunt resistance is still only about

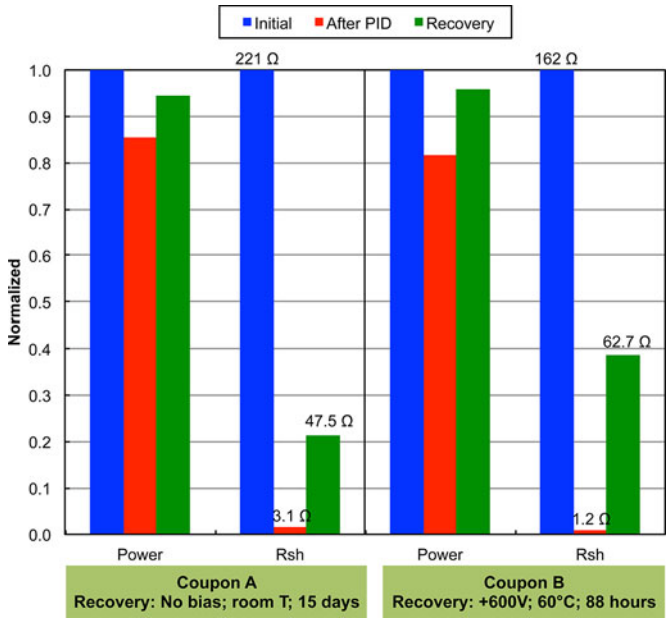

Fig. 3. Normalized power and shunt resistance. Both coupons have the same PID conditions (60 °C, −600 V, 88 h) but different recovery methods. Coupon A: 15-day room temperature storage with no bias. Coupon B: +600 V @ 60 °C, 88 h.

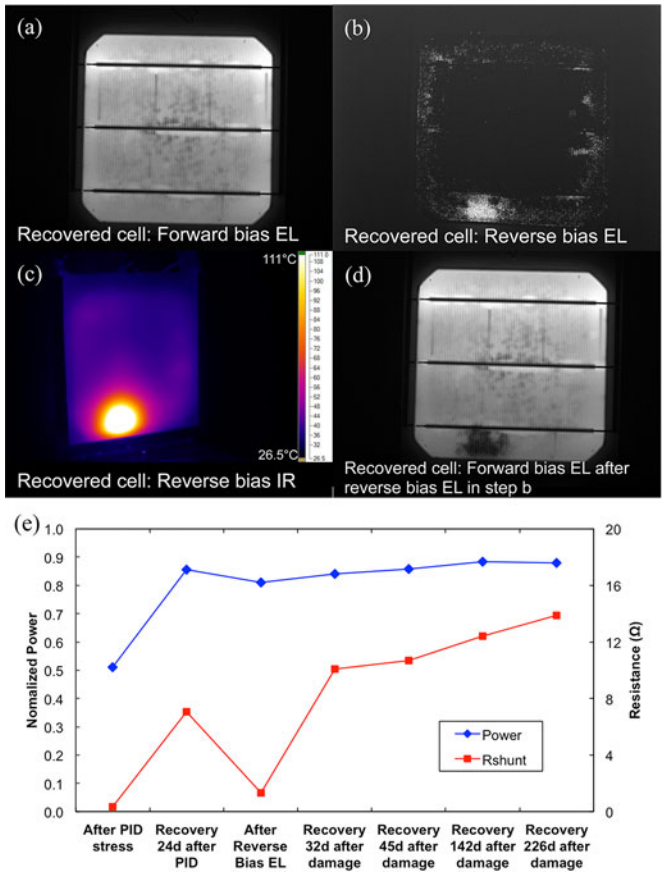

Fig. 4. EL and IR images of 24-day RT stored PID-stressed (85°C, 44 h) cell. (a) Forward-bias EL. (b) Reverse-bias EL. (c) Reverse-biased IR image. (d) Forward-bias EL after cell being damaged by reverse bias in step (b). (e) Recovery method applied for these results is the room temperature storage with no voltage application. The reverse bias imposed during EL decreased the shunt resistance. Initial R_{sh} was 183 Ω.

40% of its original. Neither of those cells showed higher than 50% shunt-resistance recovery after 125 days of room temperature storage. In addition, recovery speed for both power and shunt resistance is extremely slow after 40-day storage. This poor recovery of shunt resistance would have a serious impact on the cell efficiency at low irradiance levels [3].

This inadequate shunt resistance recovery could cause 1) a safety issue if the cells in a module were to operate under shaded/reverse-bias condition with failed bypass diodes and 2) very low energy production at the sites where the module performance primarily depends on the prevailing low-light conditions. All the fresh test coupons showed practically 0-A current flowing through the cell at −12 V. Due to cell shunting after the PID stress, the observed reverse current at −9 V was higher than 8 A just after the stress test and even after a 24-day recovery period at room temperature. Because of this localized high current in reverse bias, as shown in Fig. 4(b) and (c), the cell was found to be damaged due to high localized temperature, as shown in Fig. 4(d). The light emission (white spots) shown in the reverse bias EL image [see Fig. 4(b)] is attributed to different type of shunts (ohmic or nonohmic); in this case, shunts are caused by PID, and source of shunt can be identified by spatially resolved EL imaging with lock-in thermography under reverse and forward bias [18]. It has been reported that light emission in EL under reverse bias is also related to electrical breakdown [19]. Interestingly, it was observed that this cell was not permanently damaged, i.e., breakdown. The damaged cell was stored at room temperature for 32 days, and then, *I–V* and EL were carried out. The results, as shown in Fig. 4(e), show that there was increase of P_{max} and shunt resistance when compared with the day that cell was damaged due to reverse-bias EL measurement. EL images (not shown here) also showed a brighter damaged area than before. The cell has been monitored more than 200 days to see if there is complete recovery from PID; however, no complete recovery has been obtained. This result supports that the remaining sodium atoms in the stacking faults or the remaining sodium ions in other regions, such as SiN_x or SiO_x of the cell [20], still have a critical impact on PID-stressed cells. It is assumed that those remaining sodium atoms hinder the 100% recovery of shunt resistance and cause a very high possibility that PID-stressed cells could be easily damaged under reverse-bias condition.

Even the coupon with 92% power recovery (after 83 days at room temperature) showed a reverse current of 0.4 A at −7 V, and this localized current could be high enough in damaging the cell under reverse-bias condition. To further investigate the PID effect in terms of LIV in negative voltage, another coupon was built and PID stressed at 60 °C/−600 V/88 h. Fig. 5 shows *I–V* curves of the coupon at 240-W/m^2 irradiance level, which is a worse-performance condition for a shunted cell. There was a large reverse current after 88-h PID, while a fresh cell had no reverse current at all as shown in Fig. 5. The 98-h PID recovery of the cell (94% P_{max} at 1000 W/m^2 and 75% P_{max} at low irradiance, respectively) still showed high reverse current due

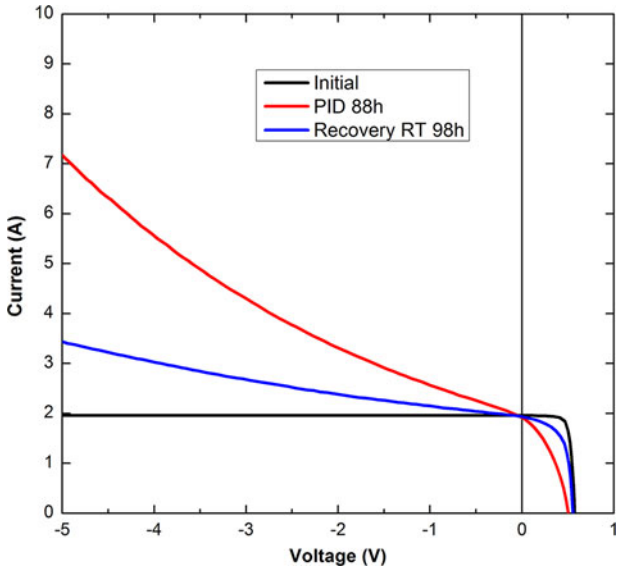

Fig. 5. *I–V* characteristics of PID-stressed and recovered cell at low irradiance (240 W/m^2) (PID 60 °C/−600 V/88 h; PID recovery at room temperature/no bias/98 h).

to very slow recovery of $R_{\rm sh}$. Therefore, it is suggested that $R_{\rm sh}$ should be monitored with $P_{\rm max}$ in evaluating PID recovery. Additionally, it was observed that the increase in reverse current is nonlinear, which represents that shunting caused by PID is not a simple shunting. The presence of localized shunts even after extensive recovery with or without reverse potential indicates the presence of traces of sodium at the junction.

B. Scaling Error of Heavily Shunted Cells

The QE measurement becomes very sensitive in the heavily shunted cells. If the series resistance of the test cell along with the input impedance of the QE system is substantial, then a significant voltage develops at the point of current generation. That voltage then drives current through the shunt in the cell, allowing less current to exit the solar cell and enter the QE system. This voltage significantly diminishes the measured QE, especially in the heavily shunted cells. The measured QE of the shunted cells will only shift up or down (scaling error) with no wavelength-dependent error. Fig. 6(a) shows QE curves, obtained at various PID recovery stages, of the same test coupon used in Fig. 2(b). It was initially thought that the large QE drop shown in Fig. 6(a) was due purely to the PID effect of the test device with no influence from the measuring equipment. When the integrated short-circuit current ($I_{\rm sc}$) from the QE curve was compared with the measured $I_{\rm sc}$ from the *I–V* curve, it was realized that there is a significant influence of test equipment on the accuracy of the QE curve. The decrease of $I_{\rm sc}$ based on the integration of the QE curve after PID is about 55%, which is a great difference than the $I_{\rm sc}$ from the conventional white LIV measurement (7%).

Since there were experimental complications in controlling the shunt resistance with high level of repeatability, a physical resistor was used to perform the simulated-PID experiments. To simulate a PID-shunted cell, an external resistor was connected

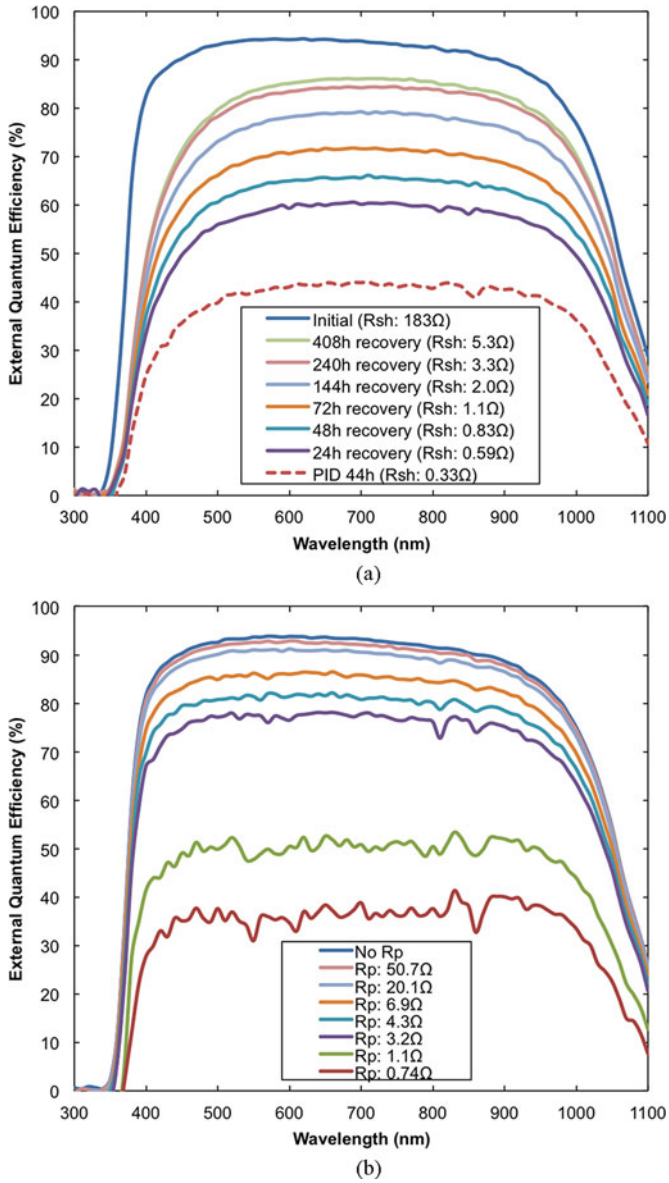

Fig. 6. (a) QE curves of same test coupon as shown in Fig. 3. (b) QE curves of a fresh cell coupon connected with various parallel resistors (R_p).

in parallel across the two leads of a fresh coupon that was not subjected to PID stress. As shown in Fig. 6(b), QE with various parallel resistances (R_p) followed the same trends as that of the PID-affected cell. This result supports that the QE drop in a PID-affected cell is not due purely to the PID effect but partly to the measuring equipment impedance as well.

To measure the QE of heavily shunted cell accurately, QE curves of the cell could be normalized, and the scaling problem could be alleviated by matching its integrated $I_{\rm sc}$ with the white light $I_{\rm sc}$ of *I–V* measurements. Another way to address this scaling problem is to make the input impedance of the QE equipment as small as possible. Therefore, an accessory having very low input impedance, developed by PV Measurements, Inc., was connected to the existing QE system. Fig. 7 shows the measured QE curves obtained without and with low impedance accessory; this figure also includes the QE curves

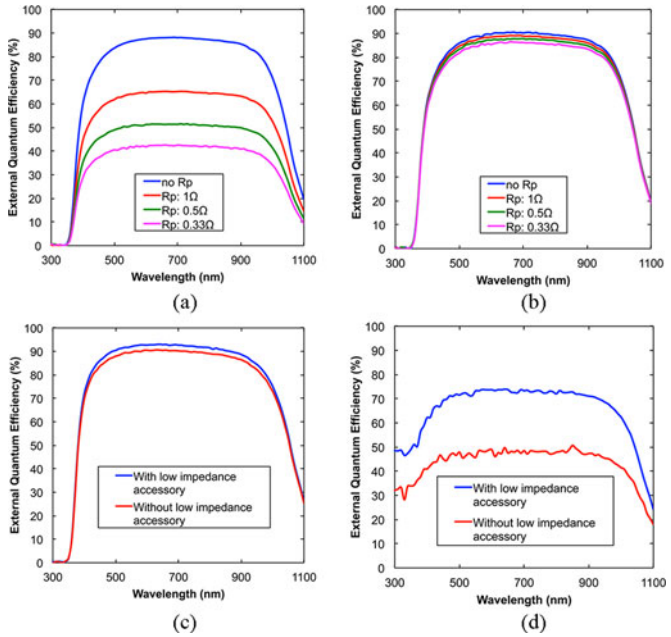

Fig. 7. Measured QE curves of a fresh cell coupon [(a) and (b)], PID cell coupon (c), and shunted cell (d). (a) Without low impedance accessory. (b) With low impedance accessory [three 1-Ω resistors were incrementally connected in parallel to the one-cell coupon leads shown in (a) and (b)]. (c) Effect of low impedance accessory on PID-affected one-cell coupon. (d) Effect of low impedance accessory on heavily shunted cell.

obtained with three 1-Ω resistors incrementally connected in parallel. On the positive side, the QE curves (with parallel resistors) with the low impedance accessory have dramatic improvements [see Fig. 7(b)] when compared with the ones without them [see Fig. 7(a)]. Therefore, it is highly recommended that QE measurements on a PID-affected cell use a QE system with low input impedance. Input impedance of QE system without the very low input impedance accessory was measured at 0.35 Ω, while the one with very low input impedance accessory is about 0.015 Ω. Measuring a severely shunted cell (e.g., $R_{\rm sh} = 1\ \Omega$) needs an input impedance smaller than 0.015 Ω in order to minimize scaling error. The use of low impedance accessory is determined to be a must for the nonintrusive QE measurements of heavily shunted PID cells connected in series in a commercial PV module [21]. The use of pulsed light bias or pulsed voltage bias method for the multijunction solar cells with low shunt resistances [22] may need to be investigated to further improve the accuracy of the existing QE system, which is already installed with the low impedance accessory.

C. Incomplete Recovery of Quantum Efficiency

Fig. 8(a) shows QE curves of coupon B, identified in Fig. 3, after PID ($P_{\rm max}$: 81%) and reverse-potential recovery ($P_{\rm max}$: 96%) steps. The QE of after-88 h-recovery stressed/shunted sample was found to be much lower than the initial due to a reason mentioned in Section III-B. To observe if the relative QE curves between the fresh/initial and recovered cell are identical, these curves were normalized. As shown in Fig. 8(a), the QE values for the photons between 350 and 600 nm wavelength are found to be lower than the QE of fresh/initial cell. This phenomenon was clearer in 85 °C PID-stressed cell, as shown in Fig. 8(b). None of the QE curves in recovery process were identical to initial ones at wavelength range from 350 to 600 nm. QE drop at short-wavelength range shows that there is another PID effect in addition to junction shunting since QE measurement of shunt-only cell affects the overall QE scale down as mentioned in Section III-B. It is well known that change of QE at short-wavelength range is caused by changes in front surface recombination velocity (FSRV) or emitter diffusion length [23]. Further details are described in Section III-D. It was shown that a huge increase in the FSRV is necessary in aligning the PID mechanism to the inversion model [24]. In addition, a degradation of front surface passivation that leads to an increase in surface recombination was observed in interdigitated back

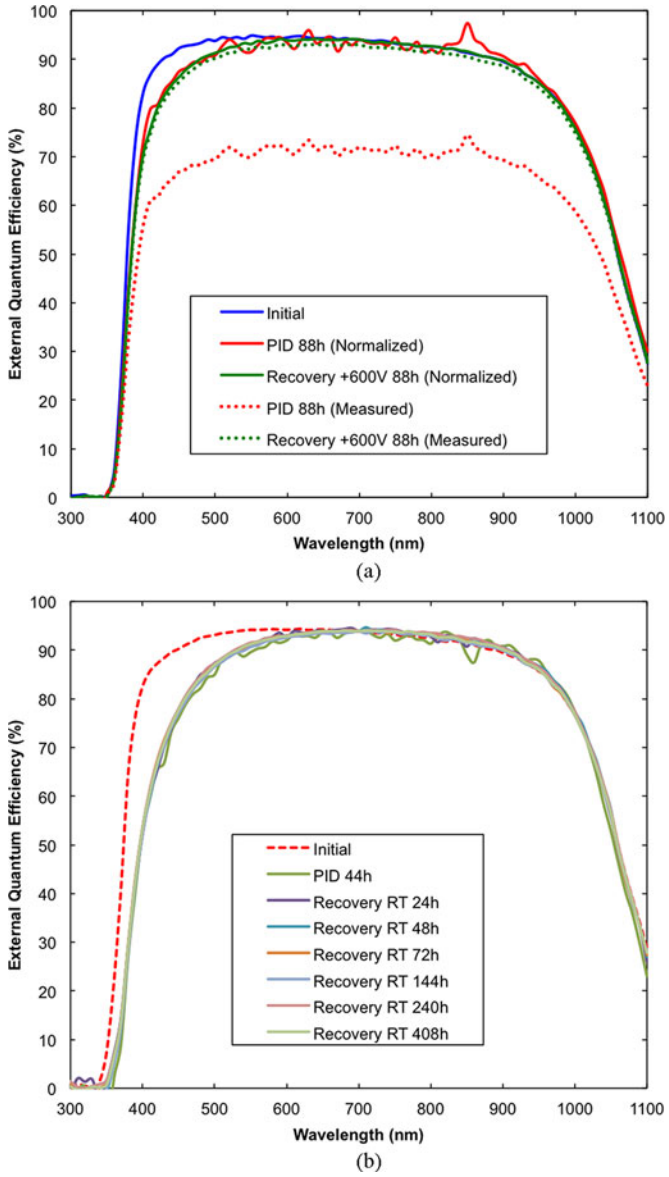

Fig. 8. (a) QE of coupon used in Fig. 3, QE of fresh/initial, PID-stressed, and recovered cells (PID stress at 60 °C/−600 V/88 h; PID recovery at 60 °C/+600 V/88 h). (b) Normalized QE of Fig. 6(a), QE of fresh/initial, PID-stressed, and recovered cells (PID stress at 85 °C/−600 V/44 h; PID recovery at room temperature (RT)/no bias/408 h).

TABLE I
PARAMETERS FOR QE PLOTS

	QE Parameters for non-PID-affected area	QE Parameters for PID-affected area
S_p (cm/s)	1×10^4	5×10^4
L_p (μm)	1	1
D_p (cm^2/s)	4	4
x_j (μm)	0.5	0.5
S_n (cm/s)	1×10^4	1×10^4
L_n (μm)	200	200
D_n (cm^2/s)	27	27
H (μm)	200	200

contact solar cells after PID stressing [25]. Therefore, PID stressed cells might possibly have a high FSRV. The mechanism for FSRV increase after PID is not fully understood, and it will be a subject of future research.

D. Quantum Efficiency Loss Modeling

The unrecovered QE or QE loss could be attributed to change of FSRV or emitter diffusion length [23], [26]. PC1D was used in simulating this effect, and QE loss shape of PID-stressed coupon in short wavelength was clearly demonstrated by either increasing FSRV or decreasing emitter diffusion length (not shown here). However, in a real PID cell, measuring area includes both PID-affected area and no/less PID-affected area due to a bigger beam size (1 mm $\times$ 5 mm) of monochromatic light in QE system than shunting spots in PID-affected area. It has been observed that PID-stressed cell has localized shunting spots, which appear circular-shaped with a diameter of 5–20 μm [8]. Since PC1D simulates the homogeneous region only, it was considered that parallel connection of no/less PID-affected area assuming low FSRV and PID-affected area assuming high FSRV were considered as a measured area. Each area of QE is obtained by using the following equations [27], and parameters used in creating these two areas are shown in Table I. To make the parallel connection of those two different areas, total QE (non-PID area + PID area) plot was calculated by multiplying a factor (for example, in this paper, PID area: 0.7 and non-PID area: 0.3 were used).

$$\mathrm{QEE} = \frac{\alpha L_p}{\alpha^2 L_p^2 - 1} \times \left[\frac{\frac{S_p L_p}{D_p} + \alpha L_p - e^{-\alpha x_j}\left(\frac{S_p L_p}{D_p}\cosh\frac{x_j}{L_p} + \sinh\frac{x_j}{L_p}\right)}{\frac{S_p L_p}{D_p}\sinh\frac{x_j}{L_p} + \cosh\frac{x_j}{L_p}} - \alpha L_p - e^{-\alpha x_j} \right] \quad (1)$$

$$\mathrm{QEB} = e^{-\alpha x_j}\frac{\alpha L_n}{\alpha^2 L_n^2 - 1} \times \left[\alpha L_n - \frac{\frac{S_n L_n}{D_n}\left(\cosh\frac{H}{L_n} - e^{-\alpha H}\right) + \sinh\frac{H}{L_n} + \alpha L_n e^{-\alpha H}}{\frac{S_n L_n}{D_n}\sinh\frac{H}{L_n} + \cosh\frac{H}{L_n}} \right] \quad (2)$$

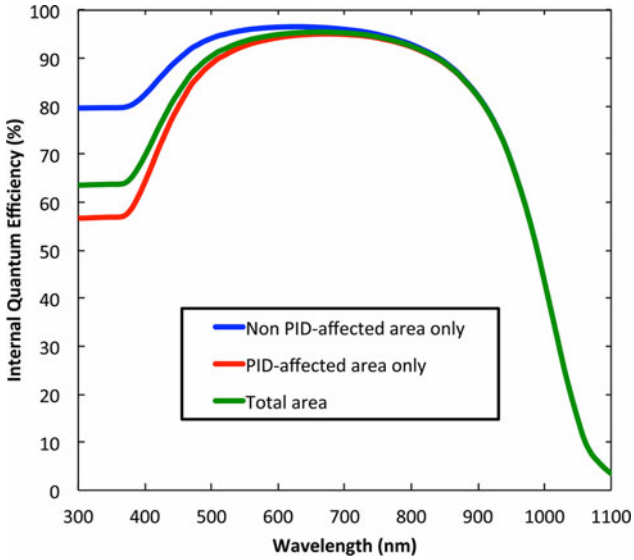

Fig. 9. Calculated QE to simulate PID-affected cell. The blue curve is based on homogeneous non-PID-affected area, the red curve is based on homogeneous PID-affected area, and the green curve is based on a combination of 70% PID affected area and 30% non-PID-affected area.

$$\mathrm{QE} = \mathrm{QEE} + \mathrm{QEB} \quad (3)$$

where

QEE QE at emitter region;
QEB QE at base region;
L_p emitter diffusion length (μm);
S_p front surface recombination velocity (cm/s);
D_p emitter diffusivity (cm^2/s);
x_j emitter thickness (junction depth) (μm);
α absorption coefficient (cm^{-1});
L_n base diffusion length (μm);
S_n back surface recombination velocity (cm/s);
D_n base diffusivity (cm^2/s);
H base thickness (μm);

Fig. 9 shows simulated QE results from the calculation mentioned above. Blue curve can be represented as QE of non-PID-affected homogeneous area. Calculated QE of PID-affected homogeneous area is shown as red curve, and it should be noticed that QE in short wavelength (300–700 nm) is decreased, as if QE of PID-stressed coupon shown in Fig. 8 is plotted. QE of total area close to real measurement also shows such QE loss shape in the short wavelength. These results indicate that a cell property could be changed by defects caused by PID in addition to change of *I–V* parameters. Based on the results presented in Section III-C, these defects leading to decrease QE in short wavelength may not be removed, although *I–V* parameters are getting slowly recovered. As shown in Fig. 9, the modeled QE at 300–360 nm is clearer in discriminating QE shifting as FSRV changes. However, QE loss from one-cell coupon, as shown in Fig. 8, has no values at such range due to cutoff wavelength (360 nm) of EVA. Therefore, it is recommended to measure QE

of PID-affected area without EVA and glass to verify this QE model.

E. Detailed Modeling of Surface Charge With Sentaurus

The previous section discussed the effect of changing surface recombination on QE. It has also been postulated that the sodium ions cause shunting though surface charge. According to proposed mechanism, the large potential difference between the cell and the frame causes a large amount of sodium to move from the glass, through the EVA encapsulant and accumulate at the surface of the solar cell. The huge amount of positively charged sodium ions at the cell surface attract the same amount of negative charges within the silicon to invert the emitter and eventually shunt the cell [17], [28]. The researchers estimated the amount of surface charges required to show the emitter inversion for typical n+ emitter with a sheet resistance of $\sim$60 Ω/square is -1×10^{15} cm^{-2}, but this number of charges was not able to be applied in PC1D [17]. We applied a different semiconductor simulation program, Sentaurus, which allows for much higher surface charge to investigate the proposed mechanism. In the modeling, typical industrial solar cell parameters were used, with a p-type base doping of 1×10^{16} cm^{-3}, a peak n-type emitter doping of 1.5×10^{20} cm^{-3}, and a junction depth of 0.5 μm. Fig. 10 shows the band diagram when surface charge of -1×10^{15} cm^{-2} was applied on an emitter surface. There was no complete surface inversion that was shown in [17]. The beginning of emitter surface started to invert; however, the inversion does not extend down to the junction region as would be required for the inversion to cause the cell to shunt. Increasing the charge further produced a similar effect to that shown in Fig. 10. The surface inverts and would change the surface recombination velocity, but the effect extends less than 10 nm into the emitter and is nowhere near the junction at 0.5 μm. Even with an unrealistically high level of -1×10^{30} cm^{-2} charge applied on the emitter surface the cell does not exhibit shunting. The Sentaurus simulation confirms the results from Saint-Cast *et al.*, who reported, by comparison of experimental and simulated DIV curves, that the inversion model cannot explain the PID shunting mechanism [24]. Therefore, a recently proposed model based on sodium decorated stacking faults [8] is preferred to the inversion model to explain the PID mechanism.

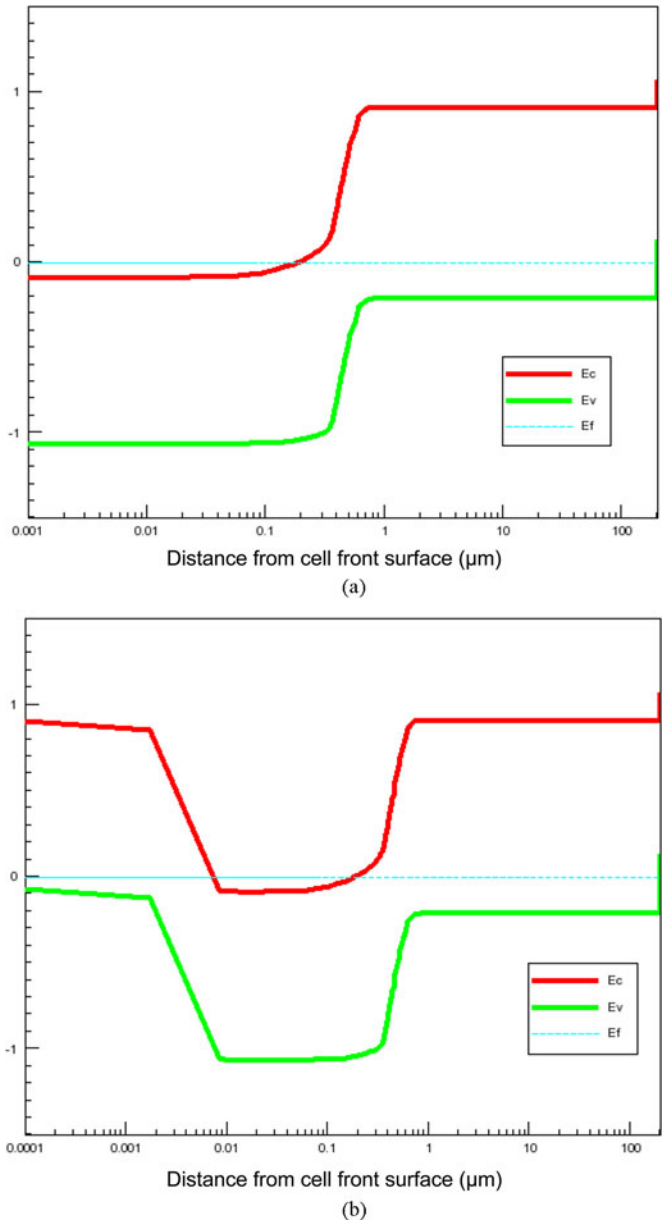

Fig. 10. Sentaurus band diagram for a solar cell. (a) No surface charge and (b) with negative surface charge (-1×10^{15} cm^{-2}).

F. Effect of Sodium Concentration in Glass on Potential-Induced Degradation

The transport of sodium from the module glass to a cell surface is strongly suspected to cause PID. Using an alternative glass with no sodium content, such as quartz, effectively protects cells in a module from PID [11], [29]. However, it is not clear that a particular amount of sodium is critical for PID. In order to further investigate the effect of sodium content in the glass on PID, two one-cell coupons using different type of glass were prepared and stressed in a condition described in Section II. The only difference is that 60 °C/85%RH was applied to the test conditions instead of using front aluminum-covered tape. The encapsulated cells were standard commercial cells known to be susceptible to PID. Coupon 1 used soda-lime glass as is typical in commercial PV modules. Coupon 2 used borosilicate glass, which has a lower sodium content than soda-lime glass and has also been shown to prevent electrochemical corrosion in thin-film modules [30]. Measurement with energy-dispersive spectroscopy (EDS) showed that primary impurity in soda-lime glass is sodium with 16% by weight. As expected, borosilicate glass has a much lower sodium content at 6.5% by weight. PID was observed in both of one-cell coupons and confirmed by *I–V* and EL. Fig. 11. shows that the borosilicate coupon is much more resistant against PID even at 100-h PID stress, while the soda-lime glass coupon was completely shunted after 24-h PID stress. These results support that sodium in a glass plays an important role in causing PID. The borosilicate glass could be used in PV modules to minimize PID, but it cannot completely protect cells from PID, and the cost would be significantly higher.

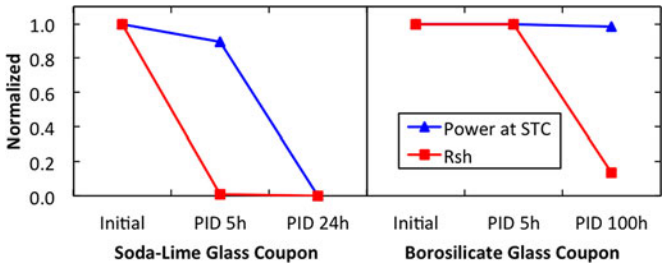

Fig. 11. PID (60 °C/85%RH, −600 V) progress of soda-lime glass coupon and borosilicate glass coupon.

IV. Summary and Conclusion

The PID-recovery methods presented in this paper show very good regeneration (up to 96%) of $P_{\max}$ at a high irradiance level of 1000 W/m^2. However, the recovery of shunt resistance and efficiency at low irradiance levels is extremely low when compared with the recovery of $P_{\max}$/efficiency at a high irradiance level. The poor cell efficiency at low irradiance levels would lead to lower energy production at predominantly low irradiance level locations and durations. The near-full $P_{\max}$ recovered cells still show much higher reverse-bias current when compared with the fresh cells. Therefore, any recovered cells/modules through the application of reverse potential and/or high temperature may pose safety risks under shaded condition if the protecting bypass diodes happen to fail in the field. Consequently, the $P_{\max}$ recovery at high irradiance level alone should not be considered as the sole parameter indicating the full recovery from the PID issue as the cells still retain some of the defects caused by the PID damage.

None of the characterization results obtained with *I–V* (dark and light), EL, and QE showed a complete recovery after the reverse potential or temperature application. QE loss in short wavelength was simulated by increasing FSRV, and it showed similar QE shape as QE of actual PID-stressed coupons. QE measurements on PID-affected bare cell from various cell manufacturers and QE mapping of whole cell surface are already in progress for further research on wavelength-dependent QE loss and PID mechanism.

The two modern commercial QE systems utilized in this study had substantial scaling error when measuring heavily shunted cells, such as PID-affected cells. The existing QE system with the low impedance accessory effectively minimizes (though not totally eliminates) QE scaling error issues in the shunted cells. Consequently, it is highly recommended to use the QE systems built with the low impedance accessory not only for the PID-related reliability research but for the solar cell design research as well.

Two different glass types (soda-lime and borosilicate glass) were utilized to determine PID effects. It was shown that borosilicate glass has a lower sodium content (6.5%) than soda-lime glass (16%) by EDS analysis and that a borosilicate glass coupon is more PID resistant than using soda-lime glass. It is concluded that sodium in glass is critical in PID effect.

Acknowledgment

The authors would like thank C. Tracy of Solar Power Laboratory for useful discussions and H. Field of PV Measurements, Inc., for the technical support and stimulating discussions.

References

[1] S. Pingel, O. Frank, M. Winkler, S. Daryan, T. Geipel, H. Hoehne, and J. Berghold, "Potential induced degradation of solar cells and panels," in *Proc. 35th IEEE Photovoltaic Spec. Conf.*, Honolulu, HI, USA, 2010, pp. 2817–2822.

[2] S. Koch, D. Nieschalk, J. Berghold, S. Wendlandt, S. Krauter, and P. Grunow, "Potential induced degradation effects on crystalline silicon cells with various antireflective coatings," in *Proc. 27th Eur. Photovoltaic Sol. Energy Conf. Exhib.*, Frankfurt, Germany, 2012, pp. 1985–1990.

[3] G. Mathiak, M. Schweiger, and W. Herrmann, "Potential-induced degradation—Comparison of different test methods and low irradiance performance measurements," in *Proc. 27th Eur. Photovoltaic Sol. Energy Conf. Exhib.*, Frankfurt, Germany, 2012, pp. 3157–3162.

[4] P. Hacke, "Considerations for a standardized test for potential-induced degradation of crystalline silicon PV modules," presented at the Photovoltaic Module Rel. Workshop, Golden, CO, USA, 2012.

[5] P. Hacke, R. Smith, K. Terwilliger, G. Perrin, B. Sekulic, and S. Kurtz, "Development of an IEC test for crystalline silicon modules to qualify their resistance to system voltage stress," *Prog. Photovoltaic Res. Appl.*, vol. 22, pp. 775–783, 2014.

[6] P. Hacke *et al.*, "System voltage potential-induced degradation mechanisms in PV modules and methods for test," in *Proc. 37th IEEE Photovoltaic Spec. Conf.*, Seattle, WA, USA, 2011, pp. 814–820.

[7] H. Nagel, A. Metz, and K. Wangemann, "Crystalline Si solar cells and modules featuring excellent stability against potential-induced degradation," in *Proc. 26th Eur. Photovoltaic Sol. Energy Conf. Exhib.*, Hamburg, Germany, 2011, pp. 3107–3112.

[8] V. Naumann *et al.*, "Explanation of potential-induced degradation of the shunting type by Na decoration of stacking faults in Si solar cells," *Sol. Energy Mater. Sol. Cells*, vol. 120, Part A, pp. 383–389, 2014.

[9] D. Lausch *et al.*, "Potential-induced degradation (PID): Introduction of a novel test approach and explanation of increased depletion region recombination," *IEEE J. Photovoltaics*, vol. 4, no. 3, pp. 834–840, May 2014.

[10] G. Mon, J. Orehotsky, R. Ross, and G. Whitla, "Predicting electrochemical breakdown in terrestrial photovoltaic modules," in *Proc. 17th IEEE Photovoltaic Spec. Conf.*, Kissimmee, FL, USA, 1984, pp. 682–692.

[11] P. Hacke, M. Kempe, K. Terwilliger, S. Glick, and S. Kurtz, "Characterization of multicrystalline silicon modules with system bias voltage applied in damp heat," in *Proc. 25th Eur. Photovoltaic Sol. Energy Conf. Exhib./5th World Conf. Photovoltaic Energy Convers.*, Valencia, Spain, 2010, pp. 3760–3765.

[12] V. Naumann *et al.*, "The role of stacking faults for the formation of shunts during potential-induced degradation of crystalline Si solar cells," *Phys. Status Solidi: Rapid Res. Lett*, vol. 7, pp. 315–318, 2013.

[13] S. Koch, J. Berghold, O. Okoroafor, S. Krauter, and P. Grunow, "Encapsulation influence on the potential induced degradation of crystalline silicon cells with selective emitter structures," in *Proc. 27th Eur. Photovoltaic Sol. Energy Conf. Exhib.*, Frankfurt, Germany, 2012, pp. 1991–1995.

[14] S. Pingel, S. Janke, and O. Frank, "Recovery methods for modules affected by potential induced degradation (PID)," in *Proc. 27th Eur. Photovoltaic Sol. Energy Conf. Exhib.*, Frankfurt, Germany, 2012, pp. 3379–3383.

[15] J. Oh, S. Bowden, and G. Tamizhmani, "Application of reverse bias recovery technique to address PID issue: Incompleteness of shunt resistance and quantum efficiency recovery," in *Proc. 40th IEEE Photovoltaic Spec. Conf.*, Denver, CO, USA, 2014, pp. 925–929.

[16] J. Oh, G. Tamizhmani, and S. Bowden, "Scaling error of quantum efficiency measurements for heavily shunted cells in reliability research," in *Proc. 40th IEEE Photovoltaic Spec. Conf.*, Denver, CO, USA, 2014, pp. 2635–2638.

[17] J. Bauer *et al.*, "On the mechanism of potential-induced degradation in crystalline silicon solar cells," *Phys. Status Solidi: Rapid Res. Lett*, vol. 6, pp. 331–333, 2012.

[18] E. Sugimura *et al.*, "Spatially resolved electroluminescence imaging of shunt sources in crystalline silicon solar cells," *Jpn. J. Appl. Phys.*, vol. 51, p. 10NA02, 2012.

[19] K. Bothe *et al.*, "Luminescence emission from forward- and reverse-biased multicrystalline silicon solar cells," *J. Appl. Phys.*, vol. 106, p. 104510, 2009.
[20] D. Lausch *et al.*, "Sodium outdiffusion from stacking faults as root cause for the recovery process of potential-induced degradation (PID)," *Energy Procedia*, vol. 55, pp. 486–493, 2014.
[21] B. Knisely, J. Kuitche, G. Tamizhmani, A. Korostyshevsky, and H. Field, "Non-intrusive cell quantum efficiency measurements of accelerated stress tested photovoltaic modules," in *Proc. 40th IEEE Photovoltaic Spec. Conf.*, Denver, CO, USA, 2014, pp. 1870–1874.
[22] J.-J. Li, S. H. Lim, and Y.-H. Zhang, "A novel method to eliminate the measurement artifacts of external quantum efficiency of multi-junction solar cells caused by the shunt effect," *Proc. SPIE*, vol. 8256, pp. 825616–1–825616-7, 2012.
[23] H. J. Hovel, *Semiconductors and Semimetals*, vol. 11. New York, NY, USA: Academic, 1975, pp. 24–37.
[24] P. Saint-Cast *et al.*, "Potential-induced degradation on cell level: The inversion model," in *Proc. 28th Eur. Photovoltaic Sol. Energy Conf. Exhib*, Paris, France, 2013, pp. 789–792.
[25] V. Naumann *et al.*, "Potential-induced degradation at interdigitated back contact solar cells," *Energy Procedia*, vol. 55, pp. 498–503, 2014.
[26] C. Honsberg and S. Bowden, *Quantum Eficiency*. (2010). [Online]. Available: http://pveducation.org/pvcdrom/solar-cell-operation/quantum-efficiency
[27] J. Nelson, *The Physics of Solar Cells*. London, U.K.: Imperial College Press, 2003, pp. 165–167.
[28] V. Naumann, C. Hagendorf, S. Grosser, M. Werner, and J. Bagdahn, "Micro structural root cause analysis of potential induced degradation in c-Si solar cells," *Energy Procedia*, vol. 27, pp. 1–6, 2012.
[29] M. Kambe *et al.*, "PID-free c-Si PV module using aluminosilicate chemically strengthened glass," in *Proc. 28th Eur. Photovoltaic Sol. Energy Conf. Exhib*, Paris, France, 2013, pp. 2861–2864.
[30] C. R. Osterwald, T. J. McMahon, and J. A. del Cueto, "Electrochemical corrosion of SnO_2:F transparent conducting layers in thin-film photovoltaic modules," *Sol. Energy Mater. Sol. Cells*, vol. 79, pp. 21–33, 2003.

Authors' photographs and biographies not available at the time of publication.